

## *Retraction*

# **Retracted: Application of Multimedia Semantic Extraction Method in Fast Image Enhancement Control**

### **Journal of Control Science and Engineering**

Received 17 October 2023; Accepted 17 October 2023; Published 18 October 2023

Copyright © 2023 Journal of Control Science and Engineering. This is an open access article distributed under the Creative Commons Attribution License, which permits unrestricted use, distribution, and reproduction in any medium, provided the original work is properly cited.

This article has been retracted by Hindawi following an investigation undertaken by the publisher [1]. This investigation has uncovered evidence of one or more of the following indicators of systematic manipulation of the publication process:

- (1) Discrepancies in scope
- (2) Discrepancies in the description of the research reported
- (3) Discrepancies between the availability of data and the research described
- (4) Inappropriate citations
- (5) Incoherent, meaningless and/or irrelevant content included in the article
- (6) Peer-review manipulation

The presence of these indicators undermines our confidence in the integrity of the article's content and we cannot, therefore, vouch for its reliability. Please note that this notice is intended solely to alert readers that the content of this article is unreliable. We have not investigated whether authors were aware of or involved in the systematic manipulation of the publication process.

Wiley and Hindawi regrets that the usual quality checks did not identify these issues before publication and have since put additional measures in place to safeguard research integrity.

We wish to credit our own Research Integrity and Research Publishing teams and anonymous and named external researchers and research integrity experts for contributing to this investigation.

The corresponding author, as the representative of all authors, has been given the opportunity to register their agreement or disagreement to this retraction. We have kept a record of any response received.

### **References**

- [1] Y. Gao, M. Chen, S. Du, and G. Feng, "Application of Multimedia Semantic Extraction Method in Fast Image Enhancement Control," *Journal of Control Science and Engineering*, vol. 2022, Article ID 2282217, 8 pages, 2022.

## Research Article

# Application of Multimedia Semantic Extraction Method in Fast Image Enhancement Control

Yuyang Gao <sup>1,2</sup>, Ming Chen <sup>1,2</sup>, Shouqing Du <sup>1,2</sup> and Guofu Feng <sup>1,2</sup>

<sup>1</sup>College of Information, Shanghai Ocean University, Shanghai 201306, China

<sup>2</sup>Key Laboratory of Fisheries Information, Ministry of Agriculture and Rural Affairs, Shanghai 201306, China

Correspondence should be addressed to Ming Chen; 1764300027@e.gzhu.edu.cn

Received 4 August 2022; Revised 15 September 2022; Accepted 1 October 2022; Published 11 October 2022

Academic Editor: Jackrit Suthakorn

Copyright © 2022 Yuyang Gao et al. This is an open access article distributed under the Creative Commons Attribution License, which permits unrestricted use, distribution, and reproduction in any medium, provided the original work is properly cited.

In order to solve the problem that it is difficult to effectively enhance the details of the compressed domain and maintain the overall brightness and clarity of the image when improving the image contrast in the current image enhancement method in the compressed domain, a multimedia semantic extraction method is applied in fast image enhancement control. It has been proposed that the algorithm that synthesizes training samples according to the Retinex model converts the original low-light image from RGB (red-green-blue) space to HSI (hue saturation intensity) color space, keeps the chrominance and saturation components unchanged, and uses DCNN to enhance the luminance component; finally, it converts the HSI color space to RGB space to get the final enhanced image. The experimental results show that the performance of the model will increase with the increase of the number of convolution kernels, but the increase of the number of convolution kernels will undoubtedly increase the amount of calculation; it can also be found that when the number of network layers is 7, the PSNR of the image output by the model increases. The highest value, increasing the number of network layers, does not necessarily improve the performance of the model; with or without BN, his training method converges more easily than direct RGB image enhancement, with higher average PSNR and SSIM values. The experimental results show that, compared with the traditional Retinex enhancement algorithm and the DCT compression domain enhancement algorithm, the algorithm has better detail enhancement and color preservation effects and can better suppress the block effect.

## 1. Introduction

Due to the interference of camera equipment, lighting conditions, and other factors in the imaging process, it is likely that the image content is not clearly recorded, there is motion blur, the color level is not obvious, noise covers up the key facts, the image resolution is reduced, and so on. When images need to be used as court evidence, news media encounter problems, which these problems may lead to the fact that the truth is buried and the facts are confused [1]. Image processing is a great way to solve visual problems. This is to select some of the user's favorite properties on the image to match the image with the naked eye, add some data, or modify the data of the original image in some way by clicking on a mask that is not needed in the image. Field features to improve the appearance of the image. In face

recognition, this technology can be used in many cases, such as those with unclear contours, blurred photos taken by illegal vehicles, and difficult-to-identify key evidence at the crime scene. However, image enhancement has changed the originality and authenticity of image data [2].

Image enhancement is mainly divided into pixel domain enhancement and compression domain enhancement. Image pixel domain enhancement was proposed in the 1980s, mainly to remap the image pixel value according to the image pixel histogram to achieve the purpose of image enhancement [3]. The enhancement of the image compression domain is proposed later than that of the image pixel domain. The main reason is to modify the DCT coefficient (DCT is the full name of discrete cosine transform) during image compression, so as to achieve the effect of image enhancement. See Figure 1.

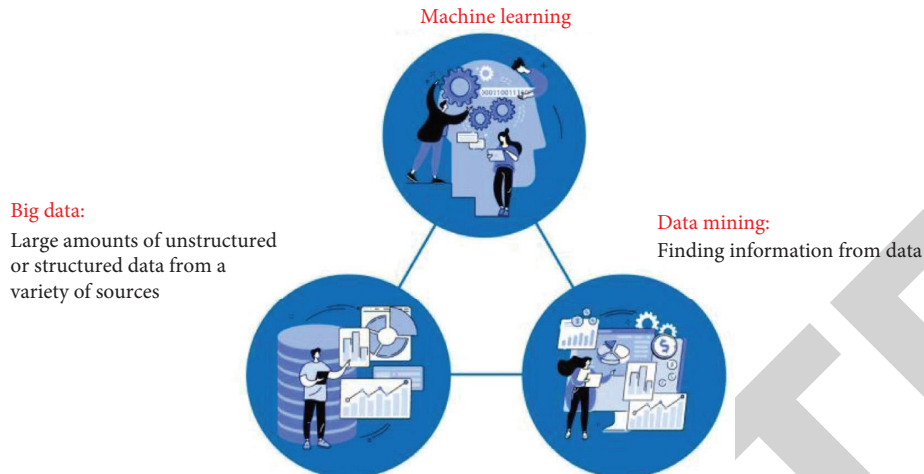


FIGURE 1: Compressed domain image.

## 2. Literature Review

Vigliocco proposed a wavelet-based homomorphic filter to enhance image contrast. The algorithm uses a homomorphic filter to process the wavelet decomposition coefficient. The processed image can not only reduce the influence of uneven illumination but also enhance the local contrast of the image [4]. Scharinger et al. combine homomorphic filtering enhancement with a neural network; a more suitable enhancement method for color images is proposed. In this method, the dynamic range is adjusted by homomorphic filtering, the contrast is enhanced, and the color of the processed image is more natural by using a neural network for color correction [5]. Pan et al. proposed a homomorphic filtering method using a spatial filtering kernel in HSI color space. This method first selects the filtering kernel according to the image size in the spatial domain and then performs homomorphic filtering in the frequency domain, which can better improve the image contrast; In addition, selecting the filtering function space in HSI space can reduce the amount of computation on the one hand, and improve the color fidelity of the processed image on the other hand [6]. Ma et al. proposed a histogram equalization algorithm based on mean segmentation. The algorithm takes the gray mean of the image as the segmentation threshold, divides the image histogram into two subhistograms, and then equalizes the two subhistograms, respectively [7]. Xu et al. proposed a local histogram equalization algorithm to maintain image brightness [8]. Jeong et al. proposed an  $\epsilon$ -filter to set a threshold for pixel comparison in the template, so that the range of low-pass filtering is narrow, the extracted incident light component is as smooth as possible, and the accuracy of illuminance estimation is improved [9]. Yang et al. proposed a Retinex algorithm for video sequences. According to the timing characteristics of video sequences, the algorithm calculates the linear correlation of different sequence images in the video to estimate the illumination. The advantages of this algorithm are simple operation and good real-time performance, which can be applied to video processing [10]. Kong et al. proposed a nonlinear filtering Retinex algorithm based on subsampling, which down

samples the low-resolution part of the image, estimates the illuminance through the nonlinear filtering of the sampled subimage, and then up samples the high-resolution part of the image to obtain the processing results, so as to speed up the operation speed of the algorithm [11, 12].

Based on the above study, this paper describes the performance of the low-illumination algorithm. This method first converts low-light images from an RGB source to an HSI (color saturation energy) color source and uses CNN (DCNN) depth to improve sharpness. Experimental results show that compared to other key algorithms, the input algorithm can not only improve sharpness and contrast but also preserve the color image data without changing it, further improving the performance of visual and objective measurements.

## 3. Research Methods

**3.1. Image Enhancement Algorithm Model.** The goal of current low-light image enhancement algorithms is to improve imageless lighting by combining the advantages of a color-changing model algorithm and CNN. First, the nonilluminated image was transferred from the RGB source to the HSI color source, then the color component  $h$  and saturation component  $s$  remained unchanged, and the lighting component  $I$  was corrected by DCNN. Finally,  $I$  converted it to RGB format to get the best picture. The operation of the conceptual algorithm is shown in Figure 2.

**3.2. Brightness Enhancement.** Unlike in-depth studies, the indirect plan uses DCNN to study the graphical relationship between endpoints between low-light and high-light images with guidance expressed in RGB settings, but only improves illumination in HSI color settings. This is because the past has changed the color of training, and practical algorithms need to be considered in order to avoid this problem, which is essential for network training.

The DCNN concept differs from the general CNN in that it has no layers or FC. The network structure consists of five components: input and output, nonlinear mapping,

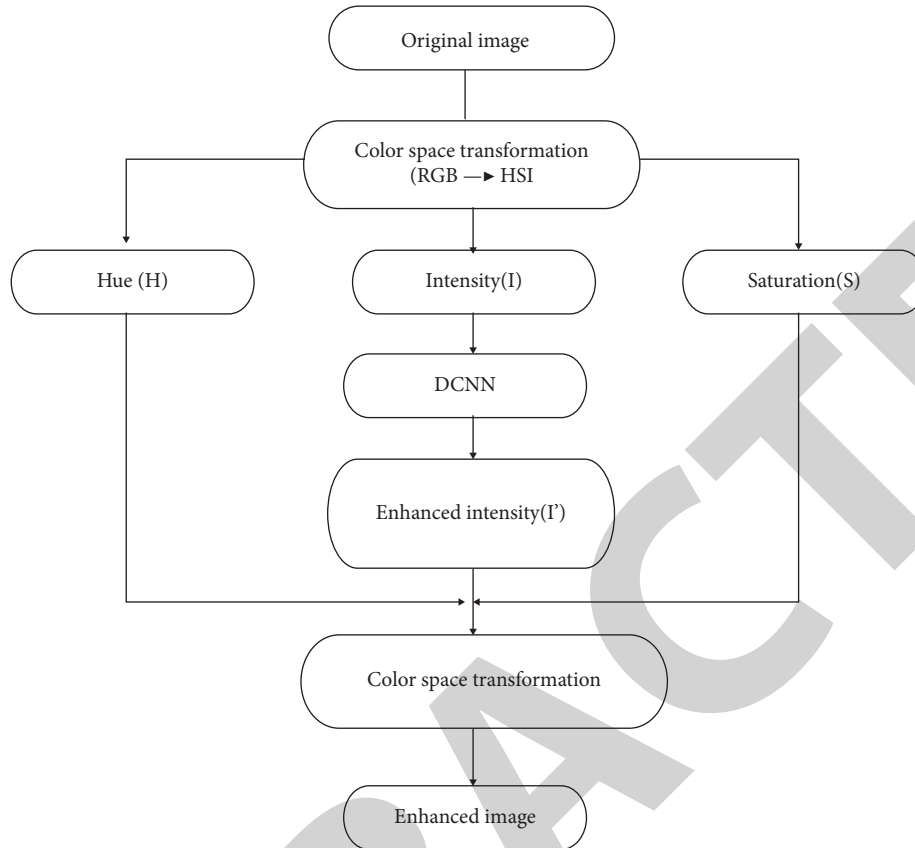


FIGURE 2: Proposed algorithm flow.

reconstruction, and output [13]. The network model in this article examines the relationship between low-light images and natural light, so it is necessary to adjust the size of the network output and the image input. The sampling process may distort large images before and after the test, which is not necessary for image processing; in addition, the rotation process can increase the image size before and after the breakdown operation and lose the data boundary. Therefore, the zero-fill operation is performed in front of all the rotating layers, which will remain the same as the image size during network transmission.

**3.2.1. Inputs and Outputs.** To better train the network, the idea, and the equipment of the network application, not the image as a whole but the similar lighting of low-light images is needed. The block was randomly selected according to the training model; at the same time, the design only improves the illumination, so the input is less bright and the output is brighter.

**3.2.2. Unpack the Feature.** The role of the first part of the network is to decompose the properties generated by the convolution layer. The transformation process is usually performed through multiple training vertebral nuclei with an input layer map or a special map of the previous layer, regardless of the characteristics of the different fields visible

by activating the nonlinear activation function [14], used to represent the features of a CNN layer map. There is a network input image block, and the feature decomposition function is shown in the following formula:

$$H_1(x) = \max(0, W_1 \times X + b_1), \quad (1)$$

where  $W_1$  is the convolution kernel, and  $b_1 \in R^{n_1}$  is the neuron bias vector. The size of  $X$  is  $n \times n$ ,  $f_1$  is the size of a single convolution kernel,  $c$  is the number of channels of the input image (only the brightness component is processed, so  $c = 1$ ), and  $\max(\cdot)$  is the maximum value. If there are  $n_1$  convolution kernels, the size of  $W_1$  is  $f_1 f_1 n_1 c$ .

After the convolution operation of the first layer of the network model and the excitation of the nonlinear function, the characteristics of different aspects of the data can be extracted from the brightness component of the low-illumination image.

**3.2.3. Nonlinear Mapping.** The nonlinear mapping is recorded as a revolutionary module, which is composed of a convolution layer, a batch normalization (BN) layer, and a ReLu (rectified linear units) excitation layer.

Let the input data set of a hidden layer of the network be  $\{\mu_1, \dots, \mu_m\}$ , and the number of samples in this batch be  $m$ . First, obtain the mean  $E(\mu)$  and variance  $D(\mu)$  of the input samples as follows:

$$E(\mu) = \frac{1}{m} \sum_{h=1}^m \mu_h, \quad (2)$$

$$D(\mu) = \frac{1}{m} \sum_{h=1}^m [\mu_h - E(\mu)]^2. \quad (3)$$

Then, normalize the batch sample data to obtain the data distribution  $\hat{\mu}_h$  with a mean value of 0 and variance of 1, i.e., the following:

$$\hat{\mu}_h = \frac{\mu_h - E(\mu)}{\sqrt{D(\mu) + \varepsilon}}, \quad (4)$$

where to avoid the denominator of the fraction being 0,  $\varepsilon$  is usually taken as a positive number close to 0.

Finally, the reconstruction parameters  $\alpha$  and  $\beta$  are introduced to reconstruct and transform the BN data, and the final output data  $z_h$  is obtained as follows:

$$z_h = BN_{\alpha, \beta}(\hat{\mu}_h) = \alpha \hat{\mu}_h + \beta. \quad (5)$$

Through nonlinear mapping, the brightness component features of the low-illumination image extracted from the first layer of the proposed network can be mapped from the low-dimensional space to the high-dimensional space, making the underlying features more abstract [14–16]. This process is expressed as the following equation:

$$H_{k-1}(X) = \max\{0, BN[W_{k-1} * H_{k-2}(X) + b_k]\}, \quad k \geq 3, \quad (6)$$

where  $k$  is the depth of the proposed network, that is, the  $k-1$  layer is the last layer of the nonlinear mapping part. It should be noted that the BN operation in the proposed network is based on the characteristic graph, not a single neuron, which can greatly reduce the  $\alpha$  and  $\beta$  introduced by the reconstruction transformation.

**3.2.4. Reconstruction.** The enhancement of low-illumination images is based on the idea of reconstruction. Reconstruction is to achieve image enhancement by minimizing the error between the brightness component of the model output and the normal illumination image through training. In this layer, reconstruction can be realized with only one convolution layer, which is described as the following equation:

$$H_k(X) = W_k \times H_{k-1}(X) + b_k. \quad (7)$$

In order to automatically learn the network model parameter  $\theta = \{W_1, \dots, W_k; b_1, \dots, b_k\}$  through training, it is assumed that the training sample set  $D = \{(X_1, Y_1), \dots, (X_\eta, Y_\eta)\}$  is given, where  $X_\eta$  and  $Y_\eta$  are the  $\eta$ -th input low-illumination image brightness component and the corresponding normal illumination image brightness component (i.e. ground truth) samples, and the objective function of the following formula is minimized by using the back propagation algorithm and the random gradient descent method.

$$L = \frac{1}{N} \sum_{\eta=1}^N \|H_k(X_\eta) - Y_\eta\|_F^2 + \lambda \sum_{t=1}^k \|W_t\|_F^2, \quad (8)$$

where  $N$  is the number of training samples;  $\lambda$  is a weight constraint term, which can prevent over fitting.

Once the optimal parameter  $\theta$  is obtained through training and learning, the network training ends. During the test, only the brightness component of a low-illumination image needs to be input, and the network model can calculate an enhanced brightness component according to  $\theta$ .

## 4. Result Analysis

**4.1. Sample Preparation.** In the experiment, a public dataset located in the blind area of the computer collected a total of 500 images from the Berkeley Segmentation Dataset with illumination based on interconnected objects (e.g., ground realities) and selected a total of 256,000 image blocks. 40 pixels  $\times$  40 pixels, then it is possible to display a low-light image after reflecting light following the distribution of similar objects. as  $S(x, y) = LR(x, y)$ .

**4.2. Experimental Setup.** The training algorithm will use Matlab r2014 as a simulation platform, and MatConvNet will receive an open-source version of the in-depth training. The computer's CPU (central processing unit) is an American Intel Core i7-7700, with a base frequency of 3.6 GHz, 16 GB of memory, and a GPU (graphics processing unit) from NVIDIA, gtx1070.

The depth of the network is 7 layers, the size of one connection is 3 pixels  $\times$  3 pixels, the number of breakdown cores for decomposing the function within the network is 64, and the size is 3 pixels  $\times$  3 pixels  $\times$  64 pixels; The total number of rotating cores in a nonlinear map section is 64, and the size is 3 pixels  $\times$  3 pixels  $\times$  64 pixels  $\times$  64 pixels; the redesign has only one integration of 3 pixels  $\times$  3 pixels  $\times$  64 pixels. The offset time of all layers of the network starts at 0; The Adam algorithm is used to train the model. The training standard is 128 and the starting value is 0.1. Each of the 10 training cycles is reduced by 1/10, for a total of 50 training cycles.

**4.3. Selection of Experimental Parameters.** To understand the performance and speed benefits, the size of all rotating kernels in this form is 3 pixels  $\times$  3 pixels, which shortens the training time and does not have a positive effect on image output [17]. As the subject and size of the conversion cores remain unchanged, this paper also provides an experimental analysis of the number of circulating cores and the number of network processes. After 50 cycles of training, the experiment was completed to obtain the correct PSNR of the images shown. The test results are shown in Table 1, where  $N1$  is the number of first circulating veins and  $NP-1$  ( $P \geq 3$ ) is the total number of circulating veins.

Refer to the configuration of the number of crashes for different processes in the SRCNN model, and select for comparison. Network standards are 3, 5, 7, and 9. As Table 1

TABLE 1: Test PSNR values under different network layers and convolution cores.

Number of layers	Number of convolution kernels	PSNR/dB
5	$n_1 = 64, n_{p-1} = 32$	21.74
5	$n_1 = 64, n_{p-1} = 64$	21.87
7	$n_1 = 64, n_{p-1} = 32$	22.23
7	$n_1 = 64, n_{p-1} = 64$	22.30
9	$n_1 = 64, n_{p-1} = 32$	22.04
9	$n_1 = 64, n_{p-1} = 64$	22.17

shows, standard performance may improve as the number of fault cores increases, but there is no doubt that an increase in the number of circulating cores increases computational costs; you can also see that the PSNR value of the model's output image is higher when the number of layers is 7. Increasing the number of network layers does not necessarily improve model performance. This is because the simple accumulation of the original network structure makes its structure unusable. Similarly, the resulting gradient dispersion will become more severe as the process intensifies.

**4.4. Experimental Analysis.** To determine the performance of the application algorithm, experiments are performed on low-light and low-light imaging images, and a comparative analysis is performed in terms of purpose and content compared to the classical algorithm. It has well-improved Dong, SRIE, and LIME algorithms in recent years.

**4.4.1. Synthetic Low-Illumination Image Experiment.** First, the synthetic low-illumination images were tested. The test samples selected live1, a public data set in the field of computer vision, to synthesize the low-illumination images. A total of 29 pictures were taken. The experimental results are shown in Table 2.

In the subjective evaluation, four images in the live1 data set are selected as examples to illustrate that Dong, SRIE, the LIME algorithms, and the proposed algorithms can enhance the synthesized low-illumination images and improve people's subjective feelings [18–20]. The proposed algorithm can not only improve the brightness and contrast of the image but also keep the color information of the image unchanged, which is closer to the original image under normal illumination. However, the proposed algorithm is still the same as other algorithms and cannot effectively enhance the dark part of the actual scene, which is a large white area. In addition, the proposed algorithm has the best enhancement effect for low-illumination images with uniform illumination, but for nonuniform illumination images, the overall brightness is slightly dark. This is because the Retinex model is still relatively simple, which is not enough to describe complex low-illumination scenes, and because the loss function used for such tasks using the depth learning algorithm is the mean square error (MSE), it cannot cover all image pixels.

In a real-world analysis of low-illumination images, the realities of the terrain are known, so we can compare the

TABLE 2: Objective evaluation indexes of different algorithms on synthetic low-illumination images.

Method	PSNR/dB	SSIM	MSE	LOE
HE	16.19	0.7985	1928.3	505
Dong	16.29	0.7947	1699.6	2040
SRIE	21.08	0.9579	686.4	776
LIME	13.47	0.8097	3230.7	1277
Proposed method	22.23	0.9204	389	402

differences in image enhancement with different algorithms and graph real-time graphs to show how the algorithm works. PSNR, structural similarity (SSIM), MSE, and LOE (lightness order error) were selected for the target measurements. Among them, the PSNR shows the image effect. The higher its value, the less distortion there is. SSIM represents the integrity of image information. The higher its value, the better the image and the similarity of the actual soil structure will be. The MSE map shows the difference between enhancement and ground reality. The higher the value, the closer the image enhancement is to the illumination of the original image. LOE generally measures the ability to hold an enhanced image well. The lower the value, the better the temporary brightness of the image and the higher the image [21]. Table 2 shows the average values of some of the measurements obtained from the live1 dataset when using different algorithms.

With the exception of SSIM, it is lower than the Sri algorithm, and PSNR, MSE, and LOE are higher than other algorithms, indicating that the desired algorithm in this form is closer to the old image with less impact. Image enhancements are more detailed and natural in nature, which determines the performance of the application algorithm.

In addition, in order to determine the effectiveness of the described process and the algorithm for directly improving the RGB image, all 50 workshop networks in this paper were trained in two control groups, four in BN, and no BN in the table. Perform the test configuration directly and record the average PSNR and SSIM obtained from the test network for each training cycle. The test results are shown in Figures 3 and 4.

It can be seen from Figures 3 and 4 that the HSI training method is easier to converge, and the average PSNR and SSIM values obtained are higher than those obtained by directly enhancing RGB images with or without BN. At the same time, it can be seen that BN can effectively improve the convergence speed of network training and obtain better results.

**4.4.2. Actual Low-Illumination Image Experiment.** The algorithmic improvements in this article apply not only to low-light imagery but also to 17 low-light images from NASA and DICM's experiments to improve low-light imaging. VV for testing. The test results are shown in Table 3.

In the case of objective analysis of real illumination images, the same image is not classified as objective observation without the use of well-illuminated images. Data

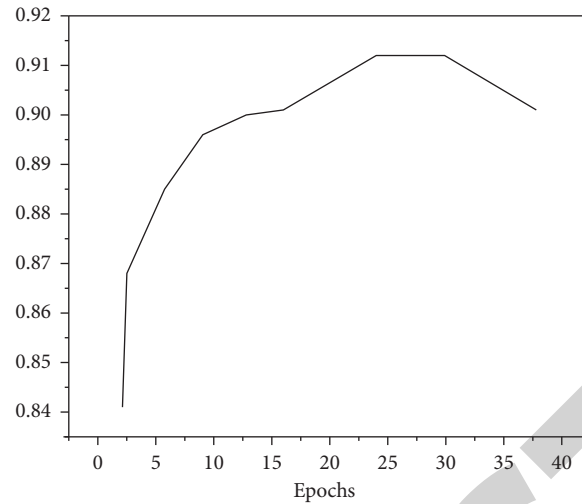


FIGURE 3: Convergence rate of HSI and RGB enhancement methods with/without BN.

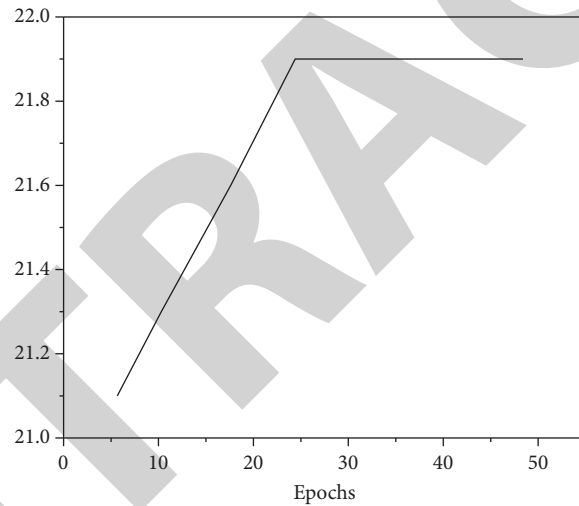


FIGURE 4: Average PSNR of 50 training cycles.

TABLE 3: Objective evaluation indexes of different algorithms on real low-illumination images.

Method	Entropy of information	Degree of chromaticity change	LOE	VIF
HE	7.1412	0.2474	571	0.4782
Dong	6.9541	0.0313	1484	0.4262
SRIE	6.9542	0.0045	972	0.6153
LIME	7.2612	0.0124	1390	0.3444
Proposed method	7.1425	0.0032	378	0.7356

entropy, degree of color shift, LOE, and optical image quality (VIF) are used to assess image quality. Of these, the entropy of the data represents the value of the image data. The larger the value, the better the image data and content are stored; the degree of chromatic aberration indicates that the color of the image is preserved. The clearer the value, the less color distortion; VIF is an excellent image analysis that combines beautiful images of patterns, image distortion patterns, and human visual system modeling. The higher the price, the

better the image quality. Table 3 shows the average values of the various objective measures after using different algorithms to improve the 17 visual effects.

It can be seen from Table 3 that the HE algorithm and the Dong algorithm have higher chromaticity change values, indicating that the color retention ability of the enhanced image is the worst because they are processed directly in the R, G, and B channels, respectively, resulting in a different increase of each color channel and color distortion. The

LIME algorithm has higher information entropy, indicating that the image obtained by this algorithm contains more information, but its LOE value is large, indicating that the brightness order of the image is damaged and the naturalness is poor. The information entropy of the SRIE algorithm is the lowest, and the detailed information is not obvious after enhancing the low-illumination image. Except that the information entropy of the proposed algorithm is lower than that of the LIME algorithm, the proposed algorithm is superior to other algorithms in the other three evaluation indexes, which shows that the image color enhanced by the proposed algorithm maintains better and has better naturalness.

## 5. Conclusion

At present, the main focus of low-light image processing algorithms is to cause color conflicts to improve sharpness and contrast. DCNN's ability to learn, such as through processing systems, to remove key data properties from large data as a whole, to adapt to hard work, and to keep chrominance components and saturation components unchanged. Based on the final concept, a map is a correlation between low-light image brightness, the best-studied image illumination, and image brightness received wonderfully. Finally, HSI moved from color space to RGB space. Experimental results show that the application algorithm not only improves brightness and contrast but also prevents color distortion. The resulting improvement is better than the current low-precision lighting algorithm, which is theoretically significant. In the future, we will continue to optimize the network structure to improve night lighting.

## Data Availability

The data used to support the findings of this study are available from the corresponding author upon request.

## Conflicts of Interest

The authors declare that they have no conflicts of interest.

## Acknowledgments

Guangdong Province Key Field R&D Plan Project "Key Technology Research and Demonstration of Land-Based Pond Smart Farms (Project No.: 2021B0202070001)."

## References

- [1] R. Souza, Y. Beauferris, W. Loos, R. M. Lebel, and R. Frayne, "Enhanced deep-learning-based magnetic resonance image reconstruction by leveraging prior subject-specific brain imaging: proof-of-concept using a cohort of presumed normal subjects," *IEEE Journal of Selected Topics in Signal Processing*, vol. 14, no. 6, pp. 1126–1136, 2020.
- [2] A. Humphries, Z. Chen, and J. Wiltshire, "Repetition priming with no antipriming in picture identification," *Vision Research*, vol. 168, pp. 9–17, 2020.
- [3] M. Chen, Y. Jin, T. Goodall, X. Yu, and A. C. Bovik, "Corrections to "study of 3d virtual reality picture quality" [jan 20 89-102]," *IEEE Journal of Selected Topics in Signal Processing*, vol. 14, no. 2, p. 472, 2020.
- [4] G. Vigliocco, A. Krason, H. Stoll, A. Monti, and L. J. Buxbaum, "Multimodal comprehension in left hemisphere stroke patients," *Cortex*, vol. 133, pp. 309–327, 2020.
- [5] C. Scharinger, A. Schüler, and P. Gerjets, "Using eye-tracking and eeg to study the mental processing demands during learning of text-picture combinations," *International Journal of Psychophysiology*, vol. 158, pp. 201–214, 2020.
- [6] Z. Pan, F. Yuan, J. Lei, W. Li, N. Ling, and S. Kwong, "Miegan: mobile image enhancement via a multi-module cascade neural network," *IEEE Transactions on Multimedia*, vol. 24, no. 99, pp. 519–533, 2022.
- [7] A. Ma, K. Sarnacki, and K. Saeed, "Binary handwriting image enhancement by directional field-guided morphology," *Information Sciences*, vol. 551, pp. 168–183, 2021.
- [8] Y. Xu, C. Yang, B. Sun, X. Yan, and M. Chen, "A novel multi-scale fusion framework for detail-preserving low-light image enhancement," *Information Sciences*, vol. 548, no. 12, pp. 378–397, 2021.
- [9] E. Jeong, J. Seo, and J. Wacker, "Grayscale drone inspection image enhancement framework for advanced bridge defect measurement," *Transportation Research Record*, vol. 2675, no. 8, pp. 603–612, 2021.
- [10] W. Yang, W. Wang, H. Huang, S. Wang, and J. Liu, "Sparse gradient regularized deep retinex network for robust low-light image enhancement," *IEEE Transactions on Image Processing*, vol. 30, pp. 2072–2086, 2021.
- [11] X. Y. Kong, L. Liu, and Y. S. Qian, "Low-light image enhancement via Poisson noise aware retinex model," *IEEE Signal Processing Letters*, vol. 28, no. 99, pp. 1540–1544, 2021.
- [12] J. Xu, Y. Hou, D. Ren et al., "Star: a structure and texture aware retinex model," *IEEE Transactions on Image Processing*, vol. 29, pp. 5022–5037, 2020.
- [13] Z. Gu, F. Li, F. Fang, and G. Zhang, "A novel retinex-based fractional-order variational model for images with severely low light," *IEEE Transactions on Image Processing*, vol. 29, pp. 3239–3253, 2020.
- [14] Y. Zhao, J. Zhang, E. Pereira et al., "Automated tortuosity analysis of nerve fibers in corneal confocal microscopy," *IEEE Transactions on Medical Imaging*, vol. 39, no. 9, pp. 2725–2737, 2020.
- [15] S. Song, J. Zhu, X. Li, and Q. Huang, "Integrate msrccr and mask r-cnn to recognize underwater creatures on small sample datasets," *IEEE Access*, vol. 8, pp. 172848–172858, 2020.
- [16] W. Wang, X. Wu, X. Yuan, and Z. Gao, "An experiment-based review of low-light image enhancement methods," *IEEE Access*, vol. 8, no. 99, p. 1, 2020.
- [17] G. Dhiman, V. Vinoth Kumar, A. Kaur, and A. Sharma, "Don: deep learning and optimization-based framework for detection of novel coronavirus disease using X-ray images," *Interdisciplinary Sciences: Computational Life Sciences*, vol. 13, no. 2, pp. 260–272, 2021.
- [18] J. Jayakumar, B. Nagaraj, S. Chacko, and P. Ajay, "Conceptual implementation of artificial intelligent based E-mobility controller in smart city environment," *Wireless Communications and Mobile Computing*, vol. 2021, Article ID 5325116, 8 pages, 2021.
- [19] J. Chen, J. Liu, X. Liu, X. Xu, and F. Zhong, "Decomposition of toluene with a combined plasma photolysis (cpp) reactor:

- influence of uv irradiation and byproduct analysis,” *Plasma Chemistry and Plasma Processing*, vol. 41, no. 1, pp. 409–420, 2020.
- [20] R. Huang, S. Zhang, W. Zhang, and X. Yang, “Progress of zinc oxide-based nanocomposites in the textile industry,” *IET Collaborative Intelligent Manufacturing*, vol. 3, no. 3, pp. 281–289, 2021.
- [21] Q. Zhang, “Relay vibration protection simulation experimental platform based on signal reconstruction of MATLAB software,” *Nonlinear Engineering*, vol. 10, no. 1, pp. 461–468, 2021.

RETRACTED